Sub-Diffraction Thermoreflectance Thermal Imaging using Image Reconstruction

Amirkoushyar Ziabari[1,2], Yi Xuan[1], Je-Hyeong Bahk[3], Maryam Parsa[2], Peide Ye[1,2], and Ali Shakouri[1,2]

1. Birck Nanotechnology Center, Purdue University, West Lafayette, IN, USA
2. Electrical and Computer Engineering, Purdue University, West Lafayette, IN, USA
3. Department of Mechanical and Materials Engineering, University of Cincinnati, Cincinnati, OH, USA

Abstract

Thermoreflectance thermal imaging technique uses light in the visible wavelength range and has a diffraction limit of ~250nm. Despite that TR is still capable of acquiring temperature signal from devices smaller in size down to ~3x below diffraction limit. Below diffraction limit, the detected thermoreflectance signal underestimates the true measured temperature by 360%. Image blurring was used in the forward problem to explain the apparent temperature of the device quite accurately. In most applications, there is no unambiguous model of the device temperature for forward problem and one needs to reconstruct the true temperature profiles of the sub-diffraction devices from their measured TR images. This is an ill-posed inverse problem which may not have a unique solution. Here, a maximum-a-posteriori (MAP) image reconstruction technique is used along with an Iterative Coordinate Descent (ICD) Optimization approach to solve this inverse problem and restore the true temperature profile of the devices. Preliminary results show that temperature of sub-diffraction heater lines down to ~150nm can be accurately estimated.

1. Introduction

Temperature is a key parameter that determines the performance and reliability of electronic and optoelectronic devices [1]–[5]. As device sizes are reduced to deep submicron scale, non-contact thermoreflectance thermal imaging (TRI) can be extremely valuable to study hot spots and the defects in integrated circuits.

TR thermal imaging is based on the change in the surface or interface reflection coefficient with temperature. As a non-contact characterization technique, and with about 250nm spatial, and 800ps temporal resolution, TR Imaging is well suited for steady-state and transient thermal characterization of electronic and thermoelectric devices [6]–[8].

TR utilized to study self-heating at the transport bottlenecks in network of silver nanowire/single layer graphene hybrid films which resulted in the observation of super-Joule self-heating effect [9]. TR was further used to map the localized alternating Peltier heating and cooling as well as Joule heating at the Metal-Insulator domain boundaries in electrically biased single crystalline VO_2 nanobeams [6]. Moreover, due to its high temporal resolution (50ns with LED, 800ps with laser [8], [10]) TR can capture fast transient self-heating effects in high speed switching devices.

While for device sizes smaller than the diffraction limit, the optical image is blurred and features are barely discernable, thermoreflectance thermal images of the same devices show clearly the thermal profile of the heated lines [9], [11]–[13]. This is due to the fact, that thermoreflectance uses lock-in technique with good signal-to-noise ratio, and because metal and semiconductor have thermoreflectance coefficients with different signs. The phase difference, akin to phase shift masks in optical lithography, can be used to identify the sharp boundaries of the heater line.

Although, TR detects thermal signals from devices below diffraction limit, the apparent measured temperature is underestimated. Diffraction blurring convolves temperature signal from nanoscale features and from those in neighboring regions, and therefore, the apparent measured temperature profile reduces. If one knows the true temperature profile, by convolving it in the reflectance domain with the right diffraction function corresponding to properties of the imaging system, the measured apparent temperature profile could be obtained.

Conversely, in practice, the true temperature profile is not known and must be estimated from its apparent measured temperature map. Since diffraction function is known, from properties of the imaging system and the wavelength of the light used, image processing techniques can be used to estimate the real temperature of the devices. In the following, a maximum-a-posteriori (MAP) image reconstruction framework is proposed to perform this reconstruction. Numerical experiments were devised and solved to demonstrate the capabilities of the proposed framework.

In section 2, experimental setup and methodologies are described. Section 3 summarizes the results for forward and inverse problem followed by conclusion in section 4.

2. Experimental setup

Device Fabrication

Molecular beam epitaxy (MBE) was used to grow 5μm of $In_{0.53}Ga_{0.47}As$ on InP substrate. The thin film was lattice matched to substrate by 100nm of $In_{0.52}Al_{0.48}As$ at interface. Next, the native oxide was removed with one-minute dilute HF solution dip and 20 nm thick Al_2O_3 insulation layer was deposited using the atomic layer deposition (ALD) technique at 200 ^{0}C. This step was followed by rapid thermal annealing at 450 ^{0}C for 30s. Subsequently metal heater lines consisting of Au (~100nm) / Ti

(5 nm) were deposited by Electron beam lithography (EBL). The metal line thickness was measured to be 90nm. A series of heater lines 10µm wide down to 100nm are fabricated. The length to width ratio of metal lines was fixed to 40. Electrical probing of the heater lines was facilitated by including four $80\times80\mu m^2$ contact pads for each heater line. These are used both for electrical biasing for TR thermal imaging, as well as to further independently confirm the temperature measurements by measuring the heater electrical resistance. A scanning electron micrograph (SEM) of a 200nm heater line is shown in Figure 1a. The corresponding vertical cross section is shown in Figure 1b.

Thermoreflectance (TR) Thermal Imaging

TR thermal imaging measures the change in the reflectance of the device under electrical bias due to temperature change. The schematic in Figure 1c illustrates the working principle of TR thermal imaging. While the device under test (DUT) is being biased by an electrical signal, a constant LED light is illuminated and the reflected light from the DUT is captured by a CCD camera. The change in reflectivity (ΔR) and the calibrated coefficient of thermoreflectance (C_{TR}) are then used to extract the temperature change of the device ($\Delta T=1/C_{TR}\,(\Delta R/R_0)$). In all the experimental results shown in this work, a 530nm illumination wavelength was used. The calibrated C_{TR} for gold and InGaAs (with ~20nm oxide on top) at 530nm under 100x objective lens is -2.3×10^{-4} and 2×10^{-4}, respectively. While the oxide is transparent to the light at visible wavelengths, it can impact the C_{TR} which is studied in [14].

Temperature dependent current voltage measurement was performed using Four-point probe technique to determine temperature dependent electrical resistivity and thermal conductivity of the gold metal lines. From this technique the average temperature change of the line at different steady-state current levels were obtained and utilized to independently extract the coefficient of thermoreflectance (C_{TR}) of the gold metal lines [12], [15]. Subsequently, these electrical resistivity and thermal conductivity of gold metal lines were used as input to finite element modeling described in the next section.

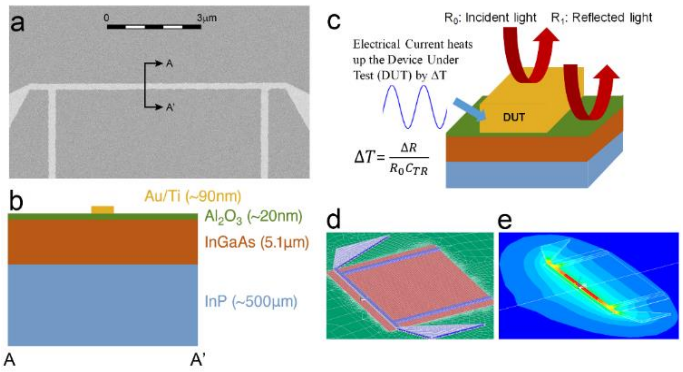

Figure 1. Device structure, experimental setup and theoretical modeling. a. Scanning electron micrograph (SEM) of a 200nm wide heater line. b. Cross section of the device structure and dimensions. c. Principle of Thermoreflectance (TR) thermal imaging. d. Computational mesh for 200nm heater line for finite element modeling (FEM) in ANSYS. e. Temperature profile of 200nm heater line obtained via FEM.

Finite element numerical modeling

ANSYS Parametric Design Language (APDL) was used to construct a finite element model (FEM) for heater lines with different diameters. Independent electrical and thermal characterization, electrical four points probe, 3ω and time domain thermoreflectance (TDTR) techniques, were used to extract electrical resistivity of the heater lines as well as thermal conductivity of different layers. These material properties along with the electrical and thermal boundary conditions were input to the FEM model. FEM meshed structure of a 200 nm heater and its corresponding temperature profile are shown in Figure 1d and 1e.

ANSYS FEM results throughout this text are compared with experimental results, and were used to verify the methodology for solving the inverse image reconstruction problem.

3. Results and discussions

Sub-Diffraction TR Thermal Imaging (Forward Problem)

According to the Rayleigh resolution criterion, also known as the diffraction limit, an imaging system cannot resolve two objects that are closer than a distance D. The distance D is proportional to the wavelength of the light used, and is inversely proportional to the numerical aperture ($N.A.$) of the imaging system ($D \sim 1.22\,\lambda/N.A.$). This distance corresponds to the radius of an Airy disc, that is point spread function (PSF) response of the imaging system, and can be appropriately modeled by a Gaussian function [13]. Figures 2a and 2b shows the CCD images of a 1µm heater line under 100x (N.A. =0.75) and 10x (N.A. =0.2) objective lenses, respectively. LED light with 530nm wavelength was used as the source for capturing this images under the microscope. This means the diffraction limit at 100x and 10x objective lenses are 0.35µm and 1.34µm. Thus, the 1µm device size is above diffraction and can be discerned at 100x (Figure 2a), while it is well below diffraction and obscured at 10x (Figure 2b).

Although diffraction sets a limit to the minimum size of the device that can be discerned, TR thermal imaging still captures thermal signals for these devices. This is evident in Figures 2c and 2d. Figures 2c and 2d show the temperature profiles for 100x and 10x measurement of the same 1µm heater line. While at 10x the device optical image is obscured (Figure 2b), its temperature profile clearly is discernable (Figure 2d). This is due to the opposite signs of the coefficient of thermoreflectance (C_{TR}) of the metal and the semiconductor. This is similar to using a 180º phase shift mask in photolithography, where the electric field sign is changed. This allows two features closer than the diffraction limit to be patterned. In TR imaging, the difference in sign of C_{TR} results in the opposite sign of reflectance change with temperature which in turn creates zero crossings near the edges of the metal and substrate, hence the signal from metal and the substrate can be distinguished.

But, what is the effect of diffraction on the accuracy of TR thermal imaging? In optical domain, images of devices below diffraction limit are filtered by the point spread function (Airy disc corresponding to the diffraction function). While in optical domain this cause the image to be obscured, in thermal domain it results in blurring of temperature profile and subsequently

reduction in the observed thermal signal. This is also evident in comparison between Figures 2c and 2d, in which the apparent temperature signal obtained under 10x objective lens is about 3x smaller than the temperature signal at 100x.

To further prove that this is the case, the following steps were taken. First the temperature profile at 100x was converted to the corresponding reflectance map knowing the nominal thermoreflectance coefficient of the materials. Next, this reflectance map is convolved with the diffraction function based on the parameters of the imaging system with 10x objective lens. The last step was then followed by converting the reflectance map back to temperature profile. This procedure is called forward modeling of the diffraction effect on TR thermal images. It is worth noting that the diffraction function is an Airy disc and can be approximated by a Gaussian function as shown in Equation 1.

$$f(r) = \frac{1}{\sqrt{2\pi}} \exp\left(-\frac{\left(\frac{2.44r}{\lambda N}\right)^2}{2}\right) \qquad (1)$$

Here, λ is the wavelength of the light and N is the focal number which is related to the numerical aperture (*N.A.*) by *1/2N.A*.

A comparison between the cross-sections of the 100x, 100x filtered (Blurred) and the 10x temperature profile results is shown in Figure 2e. This plot clearly shows that the diffraction does play a significant role in the temperature profile obtained from TR imaging for sub-diffraction devices, and by filtering the temperature profile with the correct diffraction function one can accurately predict the effect of diffraction on TR thermal images.

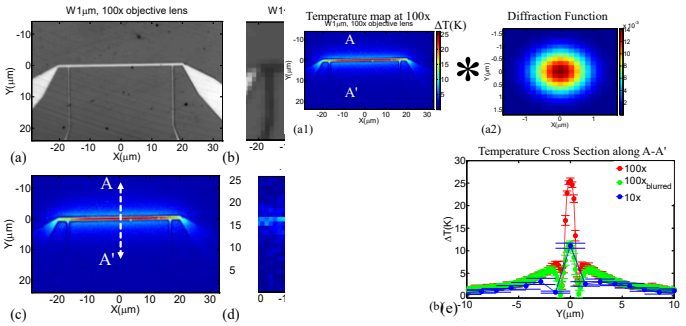

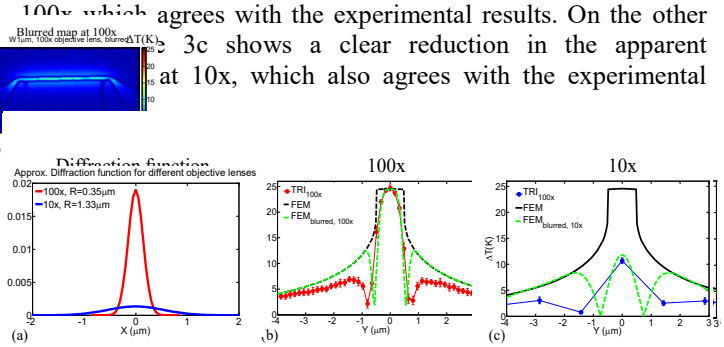

Figure 2. Optical and TR thermal image of 1μm heater line. CCD images under (a) 100x and (b) 10x objective lenses. Corresponding TR thermal images for the 1μm wide heater line under (c) 100x and (d) 10x. (e) Temperature cross sections along A-A' for 100x (red) and 10x (blue). The green curve shows that the blurring the 100x results by the diffraction function accurately matches thermoreflectance measurements with lower numerical aperture lens at 10x.

It should be pointed out, for these heater lines the average temperature and C_{TR} can independently be extracted by electrical resistivity measurement. This can be in turn used to confirm the temperature values measured optically. However, it is not always possible to have an independent sensor to calibrate for each individual heat source that is below diffraction. For example, in nanoscale transistors, is not always possible to have independent electrical measurements for features inside the transistor. In practice one needs to calibrate the thermoreflectance coefficient using larger areas on the materials or devices. It will be quite beneficial if the calibration could then be extended for small size devices that are below diffraction limit.

To examine the impact of diffraction and the forward modeling for device's temperature distribution, an accurate estimate for the true temperature profile can be determined from the FEM model. The accuracy of FEM model is demonstrated elsewhere [12]. Subsequently, the following steps will permit obtaining sub-diffraction temperature profile and compare it with the experimental results.

1. The temperature profile is obtained from the ANSYS FEM simulation.
2. Convert the temperature profile to reflectance map using the known values of the C_{TR} of metal and substrate. (calibrated bulk values)
3. The reflectance map is then blurred with the approximate optical diffraction function and then converted back to the temperature profile. This temperature profile then can be compared to the experimental results.

These steps are taken in Figures 3 and 4. Figure 3a shows cross sections of the Gaussian intensity filter simulating the optical diffraction function at 100x (red), and 10x (blue). N.A for 10x and 100x are 0.2 and 0.75, respectively. Due to smaller numerical aperture, the Gaussian filter is wider for 10x and therefore resolution is lower (1.33μm compared to 0.35μm). Figure 3b and 3c illustrate that by taking the steps 1-3 for a 1μm device and convolving the 100x and 10x filters with FEM results, the filtered response reproduces the experimental results on top of the heater very well. Figure 3b shows almost no change due to blurring at 100x which agrees with the experimental results. On the other hand, Figure 3c shows a clear reduction in the apparent temperature at 10x, which also agrees with the experimental

FEM results' cross sections at (b) 100x, and (c) 10x.

This approach is further employed to address the diffraction effect at 200nm. This is shown in Figure 4a-d. Figure 4a plots the temperature profile of the 200nm device obtained from FEM. Taking steps 1-3, the blurred results were obtained and shown above the experimental temperature profile in Figure 4b. Comparison between the cross sections shows excellent agreement for the apparent temperature at the top of the heater line between blurred numerical results and the experimental results. One should note that the difference at the tail of the temperature cross section is due to non-diffusive thermal effect and is discussed in [12]. From these simulations and experiments, one can easily conclude that the diffraction will change the

effective coefficient of thermoreflectance (C_{TR}) of the sub-diffraction size device and therefore the true temperature is underestimated using the nominal value of C_{TR}.

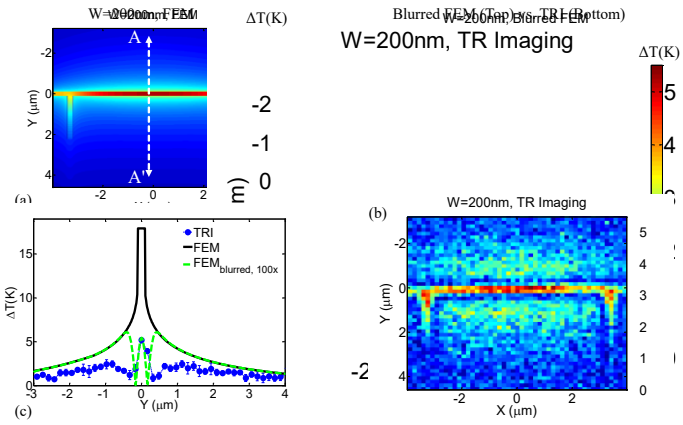

Figure 4. Comparison between experimental TR imaging, and blurred FEM temperature profile. (a) ANSYS temperature profile for the 200nm heater line. (b) Filtered result (Top) and experimental TR thermal image (bottom). TR is done with 530 nm green LED light, under 100x objective lens with N.A. = 0.75. (c) Comparison between the cross sections shows excellent agreement between experiment and filtered FEM at the top of metal line. Non-diffusive heat transport explains the difference on the tail distribution [12].

Image Reconstruction (Inversion Problem)

In many practical devices such as nanoscale transistors, one does not always have access to an independent sensor to calibrate the accurate temperature of the device under test. Instead, an apparent temperature profile of a sub-diffraction size device, the bulk values of the C_{TR} of the materials in the structure, and some knowledge about the imaging system and in turn the diffraction function, are available. The true temperature profile is needed. This is an inverse problem which is typically ill-posed and may not have unique solution.

Several techniques in image and signal processing has been developed to handle this type of inverse problems [16]. Here, a MAP estimation framework with total variation prior is proposed to solve this inverse problem. The goal is to extract the true temperature profile (f) from the measured TR thermal images (g). The following cost function in MAP framework, written in lexicographic order, needs to be minimized.

$$\hat{f} = \underset{f}{Argmin}\{\frac{1}{2\sigma_w^2}||g - \mathbf{H}f||^2 + \frac{1}{\sigma_x}\sum_{\{i,j\}\in C} S_{i,j}|f_i - f_j|\} \qquad (2)$$

Here f is the image that needs to be estimated. $\mathbf{H}$ is the filtering operator which is the diffraction function, g is the measured temperature profile, S is an averaging operator over neighboring pixels, σ^2_w is the noise variance and σ_x is the regularization parameter that balance the weight between the two terms. The first term is called fidelity term and enforces the closeness between the measured image and filtered input, while the second term (the prior model) penalizes the lack of smoothness between the neighboring pixels. The prior model is chosen to be total variation or norm-1 so that it preserves the edges and sharp boundaries [17], [18]. An iterative coordinate descent (ICD) algorithm [19] was developed to solve this optimization problem and find the minimum to the cost function. The algorithm converged typically in less than 20 iterations.

To test the proposed approach two case studies as numerical experiment were investigated. In case 1, temperature profile of 200nm heater line was obtained using ANSYS FEM. This temperature profile was then filtered with the diffraction function corresponding to the TR imaging system with 100x objective lens. Gaussian noise was added to the image so that realistic experimental results was replicated. The signal-to-noise ratio was about ~3db. This noisy-blurry temperature profile is shown in Figure 5a. Using the approach proposed in Equation 2, the temperature profile is reconstructed. This is shown in Figure 5b (Top) along with the ground truth temperature profile (bottom). Cross sections are compared in Figure 5c. Marked agreement between the reconstructed and the original temperature profiles confirms the accuracy of the proposed reconstruction technique.

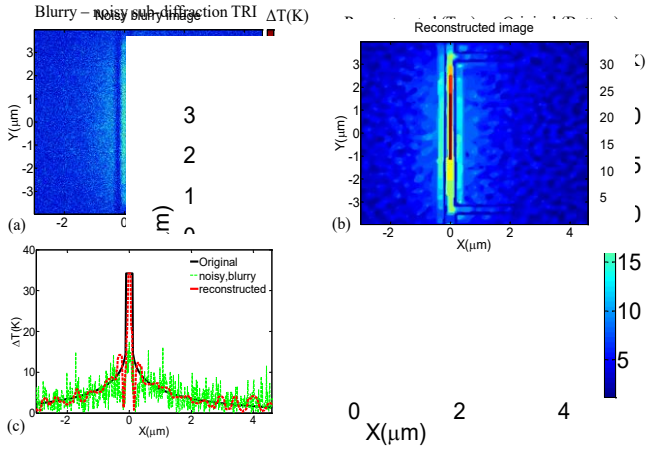

Figure 5. Image reconstruction for a 200nm single heater line case study. (a) A noisy-blurry thermal image is constructed by blurring the FEM temperature map with the diffraction function of 100x objective lens. Random Gaussian noise added to the image. (b) Reconstructed thermal image (Top) using the MAP estimation framework compared with the original temperature map (bottom) acquired by FEM. (c) Cross section comparisons along horizontal direction shows good agreement.

In the second case study, two 200nm heater lines that are separated by 1um gap are modeled using ANSYS. Temperature profile is shown in Figure 6a. Taking the same steps as the case study 1, a noisy blurry image is constructed and shown in Figure 6b. It is worth noting that the signal in the noisy-blurry image is very weak and buried in the noise (SNR ~3db). Despite that, reconstruction was performed successfully and the reconstructed image is shown in Figure 6c. Horizontal and vertical cross sections are plotted in Figure 6d and 6e. It is evident from these figures that the image reconstruction technique proposed here can be used as a powerful tool to extract the true temperature of sub-diffraction size devices.

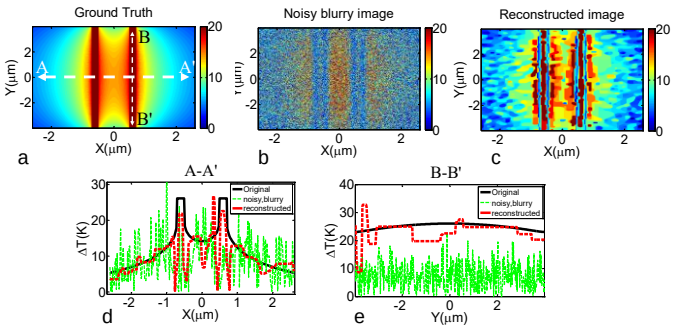

Figure 6. Image reconstruction for twin heater lines for SNR ~3db. (a-e) Ground truth, noisy-blurry, reconstructed, horizontal and vertical cross sections are shown in different columns.

To continue this work, one need to look at reconstruction of real experimental results, for which the noise variance is not known and needs to be estimated. This can be done by solving an additional ML estimate in each iteration and updating the cost function with the estimated $\hat{\sigma}_w^2$ [16]. The minimum linewidth that can reconstructed is also dependent on SNR, therefore effect of SNR of the proposed reconstruction technique needs to be investigated.

4. Conclusions

Thermoreflectance (TR) imaging as is shown to be able to measure thermal images of sub-diffraction size device using LED light in the visible range. It is elucidated that due to a change in the sign of the thermoreflectance coefficient (C_{TR}) between the metal and the semiconductor, the temperature map of sub-diffraction devices can be discerned. However, the thermal signal for objects below diffraction limit underestimate the real temperature. The effect of diffraction on TR thermal images of sub-diffraction devices is quantified. In practice, it is necessary to extract the true temperature profile from apparent measured one which is an inverse problem and typically ill-posed. To that end, a Maximum-a-posteriori (MAP) framework was developed that solves this inverse problem. Numerical experiments were designed to examine the proposed approach. Good agreement between reconstructed temperature map results, that are restored from the noisy-blurry input image data, and original thermal profile is demonstrated.

References

[1] K. Yazawa, D. Kendig, K. Maize, and A. Shakouri, "Transient therμ al characterization of HEMT devices," in *IEEE MTT-S International Microwave Symposium*, 2014, no. 1.

[2] S. H. Shin, M. Masuduzzaman, M. A. Wahab, K. Maize, J. J. Gu, M. Si, A. Shakouri, P. D. Ye, and M. A. Alaμ , "Direct Observation of Self-heating in III-V Gate-all-around Nanoωire MOSFETs," in *Electron Device Meeting, IEEE International*, 2014, vol. 2706, no. 765, pp. 510–513.

[3] L. Shi, C. Dames, J. R. Lukes, P. Reddy, J. Duda, D. G. Cahill, J. Lee, A. Marconnet, K. E. Goodson, J.-H. Bahk, A. Shakouri, R. S. Prasher, J. Felts, W. P. King, B. Han, and J. C. Bischof, "Evaluating Broader Iμ pacts of Nanoscale Therμ al Transport Research," *Nanoscale Microscale Thermophys. Eng.*, vol. 19, no. 2, pp. 127–165, 2015.

[4] S. Bhargava and E. Yablonovitch, "Loωering HAMR Near-Field Transducer Temperature via Inverse Electroμ agnetic Design," *IEEE Trans. Magn.*, vol. 51, no. 4, pp. 1–7, 2015.

[5] W. Y. Zhang, R; Zhao, W. S.; Yin, "Investigation on thermo-mechanical responses in high power multi-finger AlGaN/GaN HEMTs," *Microelectron. Reliab.*, vol. 54, no. 3, pp. 575–581, 2014.

[6] T. Favaloro, J. Suh, B. Vermeersch, K. Liu, Y. Gu, L. Chen, K. X. Wang, J. Wu, and A. Shakouri, "Direct Observation of Nanoscale Peltier and Joule E ff ects at Metal − Insulator Doμ ain Walls in Vanadiuμ Dioxide Nanobeaμ s," *Nano Lett.*, vol. 14, pp. 2394–2400, 2014.

[7] B. Vermeersch, J.-H. Bahk, J. Christofferson, and A. Shakouri, "Therμ oreflectance iμ aging of sub 100 ns pulsed cooling in high-speed thermoelectric μ icrocoolers," *J. Appl. Phys.*, vol. 113, no. 10, p. 104502, 2013.

[8] B. K. Yazawa, A. Shakouri, and P. This, "Ultrafast Subμ icron Therμ oreflectance Iμ aging," 2011.

[9] K. Maize, S. R. Das, S. Sadeque, A. M. S. Mohammed, A. Shakouri, D. B. Janes, and M. A. Alaμ , "Super-Joule heating in graphene and silver nanoωire netωork," *Appl. Phys. Lett.*, vol. 106, no. 14, p. 143104, 2015.

[10] J. Christofferson, K. Yazawa, and A. Shakouri, "Picosecond Transient Therμ al Iμ aging Using a CCD Based Therμ oreflectance Systeμ ," in *Proceedings of the 14th International Heat Transfer Conference IHTC14*, 2010, pp. 93–97.

[11] S. H. Shin, M. A. Wahab, W. Ahn, A. Ziabari, K. Maize, A. Shakouri, and M. A. Alaμ , "Fundaμ ental trade-off between short-channel control and hot carrier degradation in an extremely-thin silicon-on-insulator (ETSOI) technology," *Tech. Dig. - Int. Electron Devices Meet. IEDM*, vol. 2016–Febru, no. 765, p. 20.3.1-20.3.4, 2016.

[12] A. Ziabari et al., "Quasiballistic reduction of therμ al cross-talk in subμ icron devices," *Submitted*, 2017.

[13] A. Ziabari, J.-H. H. Bahk, Y. Xuan, P. D. Ye, D. Kendig, K. Yazawa, P. G. Burke, H. Lu, A. C. Gossard, and A. Shakouri, "Sub-diffraction Limit Thermal Iμ aging for HEMT Devices," *31th Annu. IEEE Therm. Meas. Model. Manag. Symp.*, no. 1, pp. 1–6, 2015.

[14] T. Favaloro, J.-H. Bahk, and A. Shakouri, "Characterization of the teμ perature dependence of the thermoreflectance coefficient for conductive thin filμ s," *Rev. Sci. Instrum.*, vol. 86, no. 2, p. 24903, 2015.

[15] A. Shakouri, A. Ziabari, D. Kendig, J. Bahk, Y. Xuan, P. D. Ye, S. Clara, W. Lafayette, D. Y. Peide, K. Yazaωa, and A. Shakouri, “Stable therμ oreflectance thermal imaging microscopy with piezoelectric position control,” in *2016 32nd Thermal Measurement, Modeling & Management Symposium (SEMI-THERM)*, 2016, pp. 128–132.

[16] C. a Bouman, *Model Based Image Processing*. 2013.

[17] S. Osher, A. Solé, and L. Vese, “Iμ age decoμ position and restoration using total variation minimization and the H 1 norμ s,” *SIAM Multiscale Model. Simul.*, vol. 1, no. 3, pp. 349–370, 2003.

[18] V. Caselles, A. Chaμ bolle, and M. Novaga, “Total variation in iμ aging,” *Handb. Math. Methods Imaging Vol. 1, Second Ed.*, pp. 1455–1499, 2015.

[19] C. A. Bouμ an and K. Sauer, “A unified approach to statistical tomography using coordinate descent optimization,” *IEEE Trans. Image Process.*, vol. 5, no. 3, pp. 480–492, Mar. 1996.